Adsorption (2011) 17: 5–16
DOI 10.1007/s10450-010-9267-5

MOF/graphite oxide hybrid materials: exploring the new concept of adsorbents and catalysts

Teresa J. Bandosz · Camille Petit

Received: 22 April 2010 / Accepted: 12 August 2010 / Published online: 29 August 2010

Abstract Two types of metal-organic framework (MOF)/graphite oxide hybrid materials were prepared. One is based on a zinc-containing, MOF-5 and the other on a copper-containing HKUST-1. The materials are characterized by X-ray diffraction, sorption of nitrogen, thermal analyses, Fourier Transform infrared spectroscopy (FT-IR) and scanning electron microscopy (SEM). Their features are compared to the ones of the parent materials. The water stability and ammonia adsorption capacity of the hybrid materials were also evaluated. It was found that the latter compounds exhibit features similar to the ones of the parent MOF. In most cases, their porosity increased compared to the one calculated considering the physical mixture of MOF and GO. This new porosity likely located between the two components of the hybrid materials is responsible for the enhanced ammonia adsorption capacity of the compounds. However, for both the zinc-based and the copper-based materials (MOFs and hybrid materials), a collapse of the framework was observed as a result of ammonia adsorption. This collapse is caused by the interactions of ammonia with the metallic centers of MOFs either by hydrogen bonding (zinc-based materials) or coordination and subsequent complexation (copper-based materials). Whereas the MOF-5 based compounds collapse in presence of humidity, the copper-based materials are stable.

Keywords Metal-organic frameworks · Graphite oxide · Hybrid material · Ammonia · Adsorption

T.J. Bandosz (✉) · C. Petit
Department of Chemistry, The City College and the Graduate School, City University of New York, 160 Convent Avenue, New York, NY 10031, USA
e-mail: tbandosz@ccny.cuny.edu

1 Introduction

Among the various forms of carbonaceous materials, graphite oxide (GO), also called graphene oxide or graphitic acid, has emerged as a potential precursor in synthesizing single sheets of graphene (Stankovich et al. 2006, 2007). GO is prepared by oxidation of graphite with strong oxidation agents (Brodie 1860). This treatment results in the formation of various oxygen groups (Szabo et al. 2006) on the surface and the edges of the graphene layers. Moreover, an increase in the interlayer distance from about 3 Å to 6–12 Å (Buchsteiner et al. 2006) was noticed. Because of its hydrophilic character, GO can be easily dispersed in water and other polar solvents (Park et al. 2009). The latter feature has been used to prepare two-dimensional carbonaceous sheets. In a typical method, GO is first exfoliated by dispersion in a polar solvent and then reduced chemically (Stankovich et al. 2006, 2007). GO can be also used as an adsorbent (Seredych et al. 2009), or as a component in composite materials with photochemical, conductive, adsorptive or electric property (Bissessur et al. 2006; Matsuo and Tabata 2005; Morishige and Hamada 2005; Petit and Bandosz 2009a, 2009b).

Another type of materials called metal-organic framework (MOF) has recently attracted the attention of many scientists owing to its interesting features combining both inorganic and organic solids characteristics. MOFs are formed by the "self-assembly" of metallic ions and organic ligands (mainly carboxylates and sulfonates) into regular 3D networks (Stuart 2003). This new class of materials, which exhibits very high porosity and a wide diversity of metallic centers, offers potential applications in catalysis, gas storage, gas separation and gas purification (Mueller et al. 2006). Other prospective uses include their involvement in magnetic (Konar et al. 2002) and optical devices (Pellé et al.

2007). Whereas low density of atoms in MOFs leads to their high diffusion coefficient (Stuart 2003), and is thus of interest in catalysis, it may affect the gas adsorption capacity by decreasing the retention forces, especially at supercritical conditions. The collapse of the network in the presence of water represents another issue for some MOFs (e.g. MOF-5, a zinc-based compound; Greathouse and Allendorf 2006). Finally, another problem faced by some MOF materials is their possible instability upon the removal of solvent guests during evacuation (Stuart 2003).

The preparation of hybrid materials combining MOFs and another type of material has been proposed as a solution to overcome the weak points of MOFs and to expand their field of applications (Petit and Bandosz 2009b, 2010a; Petit et al. 2010b, 2010c; Yang et al. 2009; Yoo and Jeong 2008; Yoo et al. 2009; Zacher et al. 2007). For instance, the deposition of MOFs on a substrate in order to form uniform films has been reported by Yoo and coworkers (Yoo and Jeong 2008; Yoo et al. 2009). The supports commonly used include alumina, silica or graphite (Yoo and Jeong 2008; Yoo et al. 2009; Zacher et al. 2007). Such films can enable the use of MOFs in the fabrication of membrane based separations, membrane reactors, and other advanced applications such as optical, electronic, and magnetic applications. In another field, Yang and coworkers have improved the hydrogen storage capability and water stability of MOF-5 by preparing a hybrid material combining MOF-5 and carbon nanotubes (CNTs) (Yang et al. 2009). In their material, the CNTs are incorporated inside the cubic crystals of MOF-5 but the structure of both components is preserved (Yang et al. 2009). An increase of about 40% in terms of surface area and 50% for the hydrogen storage capacity is observed for the hybrid material compared to MOF-5. Recently, we proposed to enhance the dispersive forces of MOFs by preparing MOF/GO hybrid materials and thus to improve the adsorption of small molecules such as ammonia and hydrogen (Petit and Bandosz 2009b, 2010a; Petit et al. 2010b, 2010c). GO was expected to favor the physical adsorption since, unlike MOF materials, GO is made of dense arrays of atoms. This would also lead to the formation of smaller pores which play an important role in retention processes. Two types of MOF materials were selected to build the hybrid materials. They include MOF-5 (sometimes referred to as IRMOF-1) and HKUST-1. The former material is based on zinc oxide as the saturated metallic sites and benzene dicarboxylate (BDC) as the organic linkers (Li et al. 1999). Its chemical formula is $Zn_4(H\text{-}BDC)_3$ (Li et al. 1999). The latter MOF is made of Cu^{2+} dimmers connected to oxygen atoms from benzene tricarboxylic (BTC), the organic ligand (Chui et al. 1999) and its chemical formula is $Cu_3(BTC)_2$ (Chui et al. 1999). Both MOFs are microporous adsorbents (Chui et al. 1999; Li et al. 1999). The structure of each hybrid material and its performance as ammonia adsorbents have been reported (Petit and Bandosz 2009b, 2010a; Petit et al. 2010b, 2010c).

Even though we already reported the preparation and use of the latter materials, in this paper, we propose to reintroduce and gather some of the previous findings to generalize the concept of MOF/GO hybrid materials by identifying their common features and properties. To accomplish this, in this paper, we analyze two MOF/GO hybrid materials by comparing their features according to several criteria. Their differences and similarities are discussed in terms of porosity, formation process, structural arrangement and water stability. Moreover their performance in ammonia adsorption is compared together with the mechanisms of retention involved. This comparison should provide useful criteria in the preparation of new MOF/GO hybrid materials towards specific applications in gas adsorption. This study should also draw a comprehensive understanding of the formation of MOF/GO compounds and could be used in the design of other types of MOF-based hybrid materials.

2 Materials and methods

2.1 Materials

2.1.1 Initial materials

Graphite oxide was synthesized by oxidation of graphite (Sigma-Aldrich) using the Hummers's method (Hummers and Offeman 1958). Briefly, graphite powder (10 g) was stirred with cool concentrated sulfuric acid (230 mL at 0°C). Then, potassium permanganate (30 g) was added to the suspension slowly to prevent a rapid rise in temperature (less than 20°C). The reaction mixture was then cooled to 2°C. After removal of the ice-bath, the mixture was stirred at room temperature for 30 min. Distilled water (230 mL) was slowly added to the reaction vessel to keep the temperature under 98°C. The diluted suspension was stirred for an additional 15 min and further diluted with distilled water (1.4 L), before adding hydrogen peroxide (100 mL). The mixture was left overnight. GO particles, settled at the bottom, were separated from the excess liquid by decantation followed by centrifugation. The remaining suspension was transferred to dialysis tubes (MW cutoff 6,000–9,000). Dialysis was carried out until no precipitate of $BaSO_4$ was detected by addition of $BaCl_2$. Then, the wet form of graphite oxide was centrifuged and freeze-dried. A fine brown powder of the initial graphite oxide was obtained. The resulting material is referred to as GO.

MOF-5 was prepared by mixing zinc nitrate hexahydrate (10.4 g) and 1,4 benzenedicarboxylate (2 g) in *N*,*N*-dimethylformamide (DMF, 140 mL) until complete dissolution of the solids. Then, the mixture was transferred into a round bottom flask connected to a condenser and heated at 115–120°C for 24 hours. After cooling, the supernate was

removed and crystals deposited on the bottom of the flask were collected, washed with DMF, and immersed in fresh chloroform overnight. Chloroform was changed twice during two days. Finally, crystals were collected, placed inside a closed filtering flask connected to an aspirator used to create vacuum inside the flask, and heated at 130–135°C for six hours. The resulting crystals were then kept in a desiccator.

HKUST-1 was prepared by mixing copper nitrate hemipentahydrate (10 g) and 1,3,5-benzenetricarboxylic acid (5 g) in DMF (85 mL) followed by stirring and sonication for 5 minutes. Ethanol (85 mL) was then added to the mixture, which was then stirred and sonicated for 5 minutes. Finally, deionized water (85 mL) was added to the mixture and then stirring and sonication for 30 minutes were carried out. All crystals were dissolved at this point. The mixture was then transferred to a round bottom flask (500 mL) and heated at 85°C in an oil bath. The mixture was kept in the oil bath for 21 hours under shaking (intensely for the first four hours, and then the shaking was reduced and then stopped after 20 hours). After cooling, the crystals were filtered using a Büchner funnel, washed and immersed in dichloromethane. Dichloromethane was changed twice during three days. The crystals were collected after filtration and washing with dichloromethane. Drying was then performed in vacuum using the same process as described for MOF-5. The resulting product was kept in a desiccator and is referred to as HKUST-1.

2.1.2 Hybrid materials

The hybrid materials based on MOF-5 were prepared by dispersing GO powder in the well-dissolved zinc nitrate/BDC mixture. The resulting suspensions were subsequently stirred and subjected to the same synthesis procedure as for MOF-5. The added GO consists of 5 or 20 wt% of the final material weight. The synthesized compounds are referred to as ZnMG-n with $n = 1$ and 2 depending on the GO content (5 and 20 wt%, respectively).

Similarly, to prepare the hybrid materials based on HKUST-1, GO powder was added to the well-dissolved precursors and solvents mixture used to synthesize HKUST-1. The resulting mixture was sonicated for 5 minutes, stirred for another 30 minutes and then the same synthesis procedure as that for HKUST-1 was carried out. The added GO consisted of 5 and 18 wt% of the final material weight. The compounds are referred to as CuMG-n with $n = 1$ and 2 depending on the GO content (5 and 18 wt%, respectively).

2.2 Methods

2.2.1 XRD

X-ray diffraction (XRD) measurements were conducted using standard powder diffraction procedures. The materials were ground with DMF (methanol for GO) in a small agate mortar. The mixture was smear-mounted onto a glass slide and then analyzed by CuK_α radiation generated in a Philips X'Pert X-ray diffractometer.

2.2.2 Sorption of nitrogen

Nitrogen isotherms of the samples were measured at 77 K using an ASAP 2010 (Micromeritics). Prior to each measurement, samples were outgassed at 120°C. Approximately 0.10 g of sample was used for these analyses. The surface area, S_{BET}, (BET method), the micropore volume, V_{mic}, (Dubinin-Radushkevitch method; Dubinin 1966), the mesopore volume, V_{mes}, the total pore volume, V_t, were calculated from the isotherms.

2.2.3 Thermal analysis

Thermogravimetric (TG) curves and their derivatives (DTG) were obtained using a TA Instrument thermal analyzer. The samples were heated up to 1000°C with the heating rate 10 deg/min under a flow of nitrogen of 100 mL/min.

2.2.4 FT-IR spectroscopy

Fourier transform infrared (FTIR) spectroscopy was carried out using a Nicolet Magna-IR 830 spectrometer using the attenuated total reflectance method (ATR). The spectrum was generated, collected 16 times and corrected for the background noise. The experiments were done on the powdered samples (initial and exhausted), without KBr addition.

2.2.5 SEM

Scanning electron microscopy was performed on a Zeiss Supra 55 instrument. The instrument has a resolution of 5 nm at 30 kV. Scanning was performed on a sample powder previously dried and sputter coated with a thin layer of gold to avoid charging.

2.2.6 TEM

Transmission electron microscopy (TEM) was performed on a Zeiss EM 902 instrument. The microscope has a line resolution of 0.34 nm and a point resolution of 0.5 nm and operates in normal diffraction and low dose modes at 50 or 80 kV. Analyses were performed after the samples were resuspended in ethanol.

2.2.7 NH_3 breakthrough dynamic test

In order to determine the ammonia breakthrough capacity, dynamic breakthrough tests were performed at room temperature. In a typical test, a flow of ammonia diluted with

air went through a fixed bed of adsorbent with a total inlet flow rate of 450 mL/min (225 mL/min for HKUST-1 and CuMG-n samples) and an ammonia concentration of 1000 ppm. For MOF-5 and the ZnMG-n samples, the adsorbent's bed contained about 2 cm^3 of adsorbent. In the case of HKUST-1 and the CuMG-n samples, a 2 cm^3 bed was prepared by mixing glass beads with the amount of adsorbent required to obtain a homogeneous bed (between 50 and 120 mg). This was done to avoid the pressure drop and thus to favor the kinetics of the breakthrough tests. In both cases, the mixture was packed into a glass column. The concentration of ammonia in the outlet gas was measured using an electrochemical sensor (Multi-Gas Monitor ITX system). The adsorption capacity of each adsorbent was calculated in mg per g of sorbent by integration of the area above the breakthrough curve. Tests were performed in wet conditions by diluting the ammonia stream with moist air stream, respectively. This was done to analyze the effects of water on the adsorption capacity. After the breakthrough tests, all samples were exposed to a flow of carrier air only (180 mL/min) to impose the desorption of ammonia and thus to evaluate the strength of its retention. The suffix -E is added to the name of the samples after exposure to ammonia.

3 Results and discussion

X-ray diffraction patterns of the parent and the hybrid materials (Fig. 1) provide information on their structure. The various peaks below $2\Theta \sim 7.5°$ and seen for all samples are apparent and originate from the glass slide used to run the analyses. They should not be considered in the analysis of the patterns. The two MOFs samples exhibit the expected pattern for MOF-5 and HKUST-1, respectively (Biemmi et al. 2009; Kaye et al. 2007). A single peak at about $2\Theta \sim 9.3°$ is seen in the case of GO and is related to an interlayer distance of 9.5 Å. The patterns of the hybrid materials are rather similar to the ones of the parent MOFs for both the ZnMG-n and CuMG-n series of samples. This suggests that the presence of GO did not prevent the formation of the crystalline frameworks. Moreover, it is interesting to notice that no peak corresponding to GO is present on the diffraction patterns of the hybrid materials. This is likely due to the fact that in the preparation of these materials, DMF was used. This polar solvent is known to cause the dispersion/exfoliation of GO which results in the absence of peak on the XRD patterns (Park et al. 2009). Even though the structure of each MOF is preserved in both types of hybrid materials, one can see that a splitting of the peak at about 9.7° is observed for the ZnMG-n samples and becomes more pronounced as the GO content increases. This splitting has already been described in the literature and is assigned to a

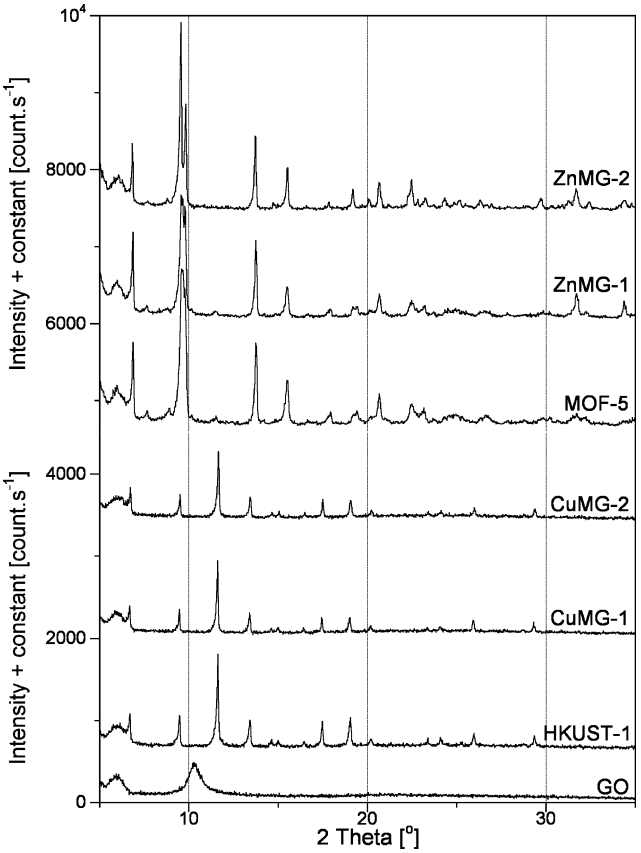

Fig. 1 X-ray diffraction patterns before exposure to ammonia for the parent materials, the ZnMG-n and CuMG-n series of hybrid materials

distortion of the cubic symmetry in MOF-5 (Hafizovic et al. 2007) which, in our case, is likely caused by the presence of GO. The frameworks of HKUST-1 does not seem affected by GO.

Porosity is a paramount feature of adsorbents. The parameters of the porous structure are listed in Table 1 and the nitrogen isotherms are plotted in Fig. 2 for all materials. In Table 1, both the structural parameters measured and the hypothetical ones calculated assuming the physical mixture of MOF and GO are listed. As seen from Fig. 2, both the MOFs and the hybrid materials of each series of samples exhibit type I isotherms typical of microporous materials. This was expected since the MOF-5 and HKUST-1 networks are made of 8 and 9 Å square channels, respectively (Chui et al. 1999; Li et al. 1999). From a general point of view, the ZnMG-n series of samples is less porous than the CuMG-n one. This must be related to the lower porosity of MOF-5 compared to HKUST-1. It is interesting to notice that CuMG-1 and CuMG-2 have a higher surface area and volume of pores than HKUST-1. Moreover, one can notice that for the CuMG-n samples, the measured porosity is always higher than the hypothetical one. This enhanced porosity is likely due to the creation of new pores at the interface between the MOF component and the GO component. On the contrary,

Table 1 Parameters of porous structure derived from nitrogen isotherms and the hypothetical values (H) calculated assuming the physical mixture between the hybrid materials components

Sample	S_{BET} [$m^2\ g^{-1}$]	V_{tot} [$cm^3\ g^{-1}$]	V_{meso} [$cm^3\ g^{-1}$]	V_{mic} [$cm^3\ g^{-1}$]	$\frac{V_{mic}}{V_{tot}}$	$S_{BET}H$ [$m^2\ g^{-1}$]	$V_{tot}H$ [$cm^3\ g^{-1}$]	$V_{mic}H$ [$cm^3\ g^{-1}$]
GO	5	na	na	na	–	–	–	–
MOF-5	793	0.41	0.02	0.39	0.94	–	–	–
ZnMG-1	706	0.37	0.03	0.34	0.93	753	0.39	0.37
ZnMG-2	603	0.33	0.04	0.29	0.89	634	0.33	0.31
HKUST-1	909	0.47	0.02	0.45	0.95	–	–	–
CuMG-1	989	0.52	0.04	0.48	0.93	864	0.45	0.43
CuMG-2	996	0.57	0.05	0.52	0.92	746	0.39	0.37

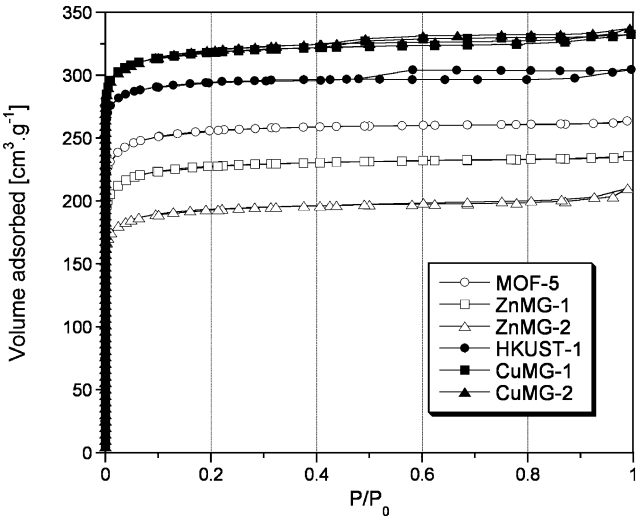

Fig. 2 Nitrogen isotherms at 77 K before exposure to ammonia for the parent materials, the ZnMG-n and CuMG-n series of hybrid materials

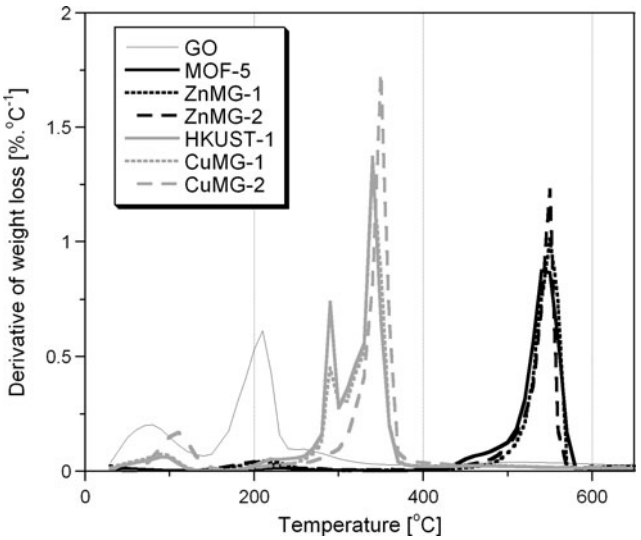

Fig. 3 DTG curves before exposure to ammonia for the parent materials, the ZnMG-n and CuMG-n series of hybrid materials

the porosity of the ZnMG-n samples is smaller than that of MOF-5 and than that one calculated for the physical mixture of MOF and GO. That smaller volume of pores does not contradict the existence of enhanced dispersive forces, which will be discussed later in this paper.

Thermal analyses results, presented in Fig. 3, provide some indications on the formation of the new hybrid materials. The DTG curve for GO reveals a major peak at ∼200°C related to the decomposition of epoxy groups (Lerf et al. 1998). The smaller peak below this temperature is due to the removal of physically adsorbed water whereas the one above 250°C represents the decomposition of carboxylic and sulfonic groups (Szymanski et al. 2002). Similar as in the cases of X-ray diffraction and nitrogen adsorption analyses, the features of the hybrid materials resemble to the ones of the parent MOFs for both the ZnMG-n and the CuMG-n series of samples. In the case of MOF-5 and ZnMG-n samples, the small peak at ∼200°C is attributed to the removal of solvent (Huang et al. 2003). For the HKUST-1 and CuMG-n samples, water is released at ∼100°C. Decomposition of the organic ligand (BDC or BDC) with release of CO_2 and collapse of the MOF structure is observed at ∼540°C for the MOF-5 and ZnMG-n samples and 350°C for the HKSUT-1 and CuMG-n samples. This indicates the greater thermal stability of the zinc-based materials than that of copper-based ones. The peak at ∼300°C for the latter materials is assigned to the release of water of crystallization (Seo et al. 2009). The decrease of that peak in the hybrid materials when GO is present can be due to a decrease in surface hydrophilicity. An explanation for that could be in the involvement of the oxygen groups in GO in linkages with the MOF component. Indeed, if these linkages are formed, then MOFs units are surrounded by carbon layers (from GO) creating a hydrophobic environment around the MOF units and thus resulting in an apparent decrease in hydrophilicity. In fact, an interesting feature of the hybrid materials is the absence of the intense peak of GO related to epoxy groups. This suggests that these functionalities are involved in the building

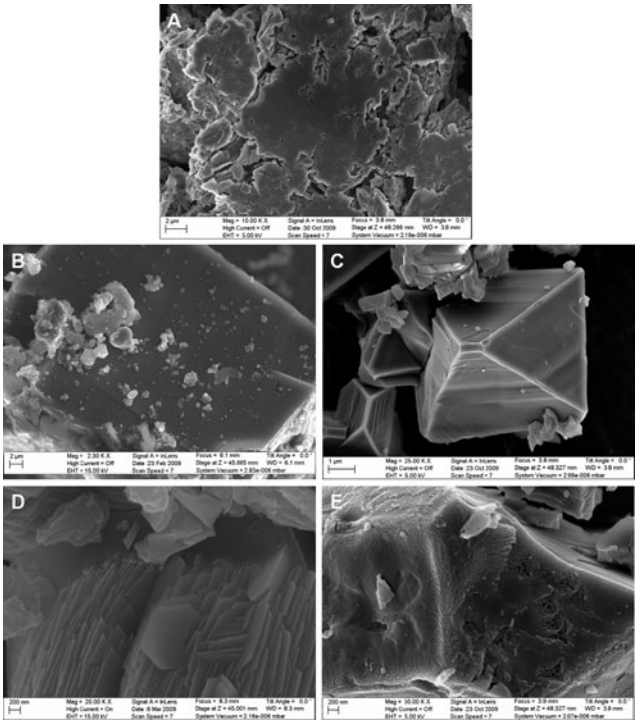

Fig. 4 SEM pictures of (**A**) GO, (**B**) MOF-5, (**C**) HKUST-1, (**D**) ZnMG-1 and (**E**) CuMG-2

process of the new materials. To verify that the absence of this peak was not due to the reaction of the epoxy groups with compounds other than HKUST-1 during the synthesis of the hybrid materials, we subjected GO alone to the same synthesis process as for the hybrid materials and run thermal analyses on the resulting sample. The above hypothesis was supported by the presence of the peak at 200°C on the DTG curves for these materials. In fact the formation of MOF occurs via the coordination of carboxylates groups (and thus oxygen groups) and metallic centers. Among the functionalities of GO capable of binding the metals sites, one can mention epoxy, carboxylic, hydroxylic and sulfonic groups.

SEM pictures of the parent and the hybrid materials are presented in Fig. 4. For the two series of samples, small differences in the texture of the hybrid materials compared to that of the parent materials can be seen. In the case of GO, we observe a dense packing of carbon layers whereas both MOF-5 and HKUST-1 exhibit crystalline structures with some defects (and remains of an amorphous phase for MOF-5). The ZnMG-1 sample appears as a layered compound. These layers likely correspond to an alternation between layers of GO and MOF-5 blocks. The overall texture of the CuMG-n samples differs from the other type of hybrid materials as seen on the SEM image of CuMG-2.

TEM images of MOF-5, GO and ZnMG-2 are presented in Fig. 5. MOF-5 particles appear in Fig. 5A. In the case of GO, well-defined carbon layers are observed (Fig. 5B).

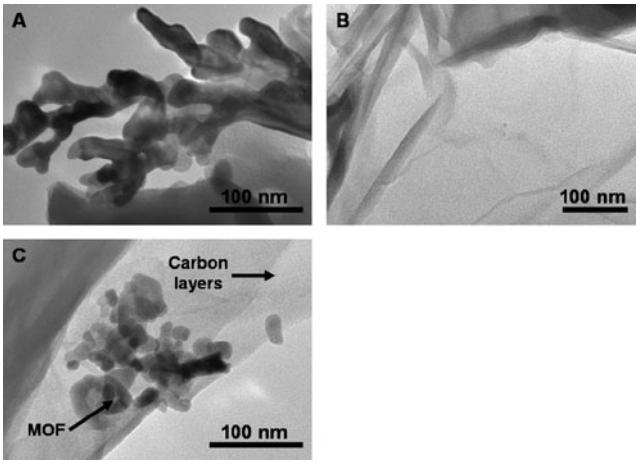

Fig. 5 TEM pictures of (**A**) MOF-5, (**B**) GO, and (**C**) ZnMG-2

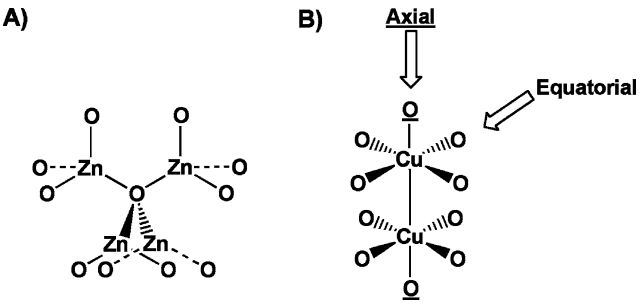

Fig. 6 Oxygen coordination sites available in (**A**) MOF-5 and (**B**) HKUST-1

For ZnMG-2 sample (Fig. 5C), carbon layers with embedded MOF-5 units are visible. These pictures show that the MOF and GO component are well-mixed within the hybrid materials. This supports the results of thermal analyses and the hypothesis that chemical interactions are involved in the formation on the composites. Similar observations can be made for the copper-based samples (images not shown here).

Considering the differences between the two series of hybrid materials and taking into account the data from thermal analyses, we believe that the formation of the materials is governed by availability of the oxygen groups of GO and the way they are coordinated to the metallic sites. In the case of MOF-5, all the oxygen atoms forming the zinc oxide tetrahedra are equivalent in terms of "spatial arrangement" (see Fig. 6). Consequently, any change of structure between the ZnMG-n samples must be related to the oxygen groups of GO. GO contains oxygen groups on the basal planes (epoxy, hydroxyl, ketone ...) and on the edges of the layers (carboxylic and sulfonic groups). Depending on the type of groups interacts with MOF-5 metallic sites, the structure of the hybrid materials can change. For instance with a high GO content, more carboxylic groups are present and their interaction with zinc must be preferred compared

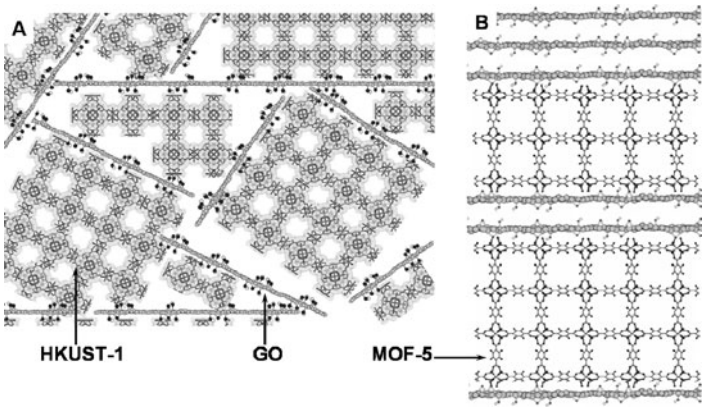

Fig. 7 Envisioned structures for the hybrid materials based on (**A**) MOF-5 and (**B**) HKUST-1

to the epoxy groups. This is because, besides the numbers of groups, one can also consider the probability for the MOF units/precursors to "encounter" the GO functional groups in the synthesis medium. As the content of GO increases, this probability increases for both carboxylic and epoxy groups. Given the preferred affinity of copper for carboxylic groups (compared to epoxy), we think that, at some point (for a specific GO content), the binding copper/carboxylic groups can be dominant. This overall mechanism of hybrid materials formation is also applicable to the CuMG-n samples. However, in this case an additional "degree of modification" must be taken into account since the coordination to the copper sites are not all equivalent. Indeed, attachment of the oxygen groups of GO to copper can occur either in the axial position (replacement of water molecule) or in the equatorial position (replacement of BTC) (see Fig. 6). Because of this, one might expect a more disordered structure in the case of CuMG-n samples compared to the ZnMG-n materials. One has to remember that this ordered/disordered character refers to the molecular structure of the materials and is not necessarily apparent in the SEM images.

Considering all the above, proposed structures for the ZnMG-n and CuMG-n samples are shown in Fig. 7. The more regular arrangement of the MOF-5-based compounds and their layered structure is visualized. On the contrary, the copper-based hybrid materials exhibit a more disordered structure. These two representations are therefore in agreement with the SEM images and the expected interactions between MOF metallic centers and the oxygen groups of GO. Moreover, in both series of samples, a new pore space is created between the MOF blocks and the GO units.

The hybrid materials were tested for the ammonia removal in moist conditions and Fig. 8 shows the breakthrough and desorption curves obtained for all samples. As seen from the shape of the breakthrough curves, the kinetics of interactions between ammonia and the hybrid materials are faster for the HKUST-1 based materials than for the zinc-containing compounds. Moreover, for both types of hybrid materials and MOFs, the retention of ammonia is

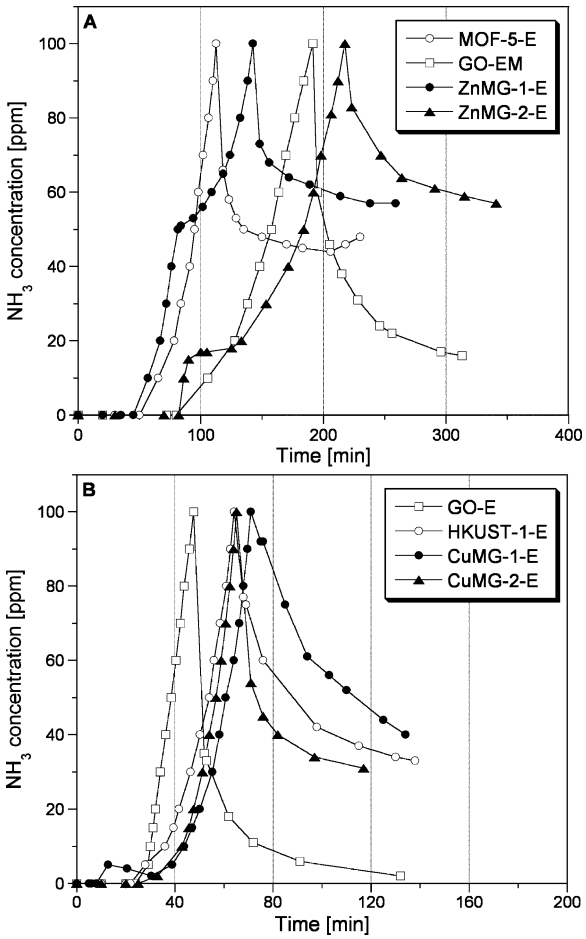

Fig. 8 Breakthrough and desorption curves for GO, the zinc-based (**A**) and the copper-based materials (**B**)

rather weak as can be seen from the shape of the desorption curves. The weakly adsorbed ammonia released during air purging must be the one dissolved in the water film formed in the adsorbents pore space (Petit and Bandosz 2009c). An interesting plateau is noticed on the breakthrough curves on the ZnMG-n samples. The concentration at which this plateau appears decreases with the in-

Table 2 Ammonia breakthrough capacities (measured and hypothetical) for the parent materials and the hybrid materials

Sample	NH_3 breakthrough capacity [mg/g of adsorbent]	
	Measured	Hypothetical
GO	61	–
MOF-5	43	–
ZnMG-1	53	43
ZnMG-2	80	46
GO	33	–
HKUST-1	172	–
CuMG-1	200	165
CuMG-2	182	147

crease in the GO content. This feature has already been observed for another MOF tested for ammonia removal but no explanation was proposed (Britt et al. 2008). It can be related to the appearance of new centers able to interact with ammonia. The adsorption capacities determined from the breakthrough curves are listed in Table 2 for all the samples together with the hypothetical adsorption capacities. The latter correspond to the adsorption capacities of the physical mixture of MOF and GO. It is worth noticing that in the case of ZnMG-n samples, the component showing the best ammonia adsorption capacity is GO whereas it is the MOF material in the case of HKUST-1 (Table 2). The difference in the breakthrough capacities between MOF-5 and HKUST-1 and consequently, the ones of the corresponding hybrid materials, can be partially attributed to the fact that in MOF-5, contrary to HKUST-1, the metallic sites are saturated. As a result of this, ammonia is able to bind directly to the copper sites of HKUST-1, which enhances the adsorption. As seen from Table 2, the measured adsorption capacities of the hybrid materials are always higher than the ones calculated for the physical mixture, thus indicating a synergetic effect between the MOF component and GO. This synergetic effect is the result of the presence of the new pore space developed in the hybrid materials where the dispersive forces are enhanced compared to MOF due to the presence of GO.

To analyze the mechanism(s) of adsorption and their effect(s) on the adsorbents structure, the exhausted samples were analyzed by various techniques and the data obtained are compared to the ones found for the initial samples. We stress more on the new features observed in the MOF samples and the hybrid materials than in the GO sample. This does not imply that the GO is not involved in the adsorption process. On the contrary, ammonia retention on GO can be high and has already been described in the literature (Petit et al. 2009d). Consequently, only the main features of this adsorption are reintroduced here. Figure 9 presents

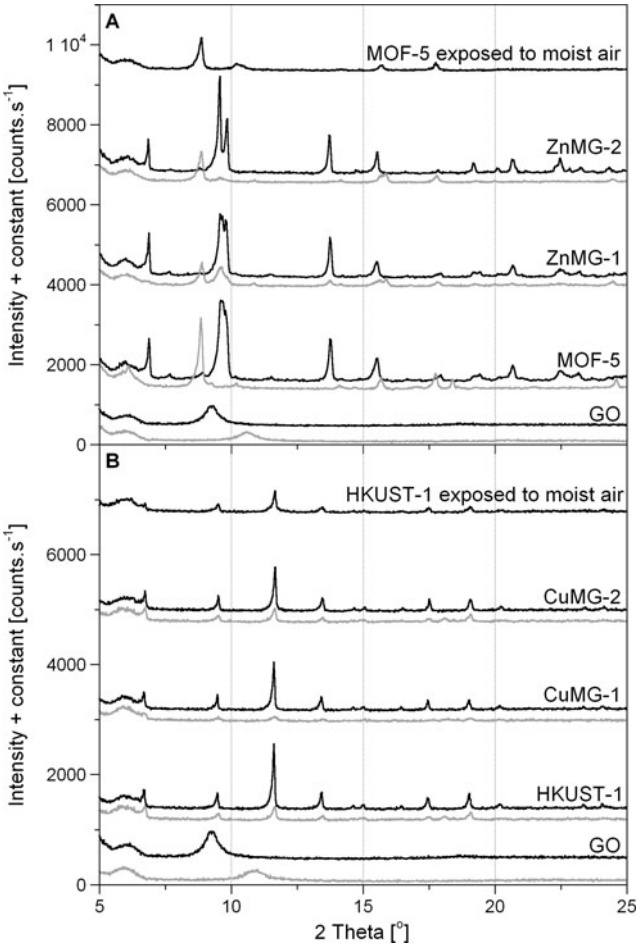

Fig. 9 X-ray diffraction patterns before (*black line*) and after ammonia adsorption (*gray line*) for GO, the zinc-based (**A**) and the copper-based materials (**B**)

the X-ray diffraction spectra of the samples before and after exposure to ammonia. Ammonia adsorption causes changes in the structure of the materials (Fig. 9). For the GO sample, a decrease in the interlayer (shift of the peak at higher Theta values) is observed. As found in a previous study, this decrease is related to the fact that ammonia react with the functional groups of GO present on basal planes (epoxy groups) and at their edges (sulfonic) (Petit et al. 2009d). These reactions result in bond cleavages which lead to a more efficient staking of the graphene layers and thus a decrease of the interlayer distance (Petit et al. 2009d). For all exhausted zinc-based samples, a complete modification of the XRD pattern is observed indicating the collapse of the MOF structure. The resulting spectra look like the one of MOF-69c (Rosi et al. 2005). In the latter study, the destruction of MOF-5 was related to the hydrogen bonds between water and the zinc oxide tetrahedra. Due to the similar chemistry of the water and ammonia molecules, it can be hypothesized that the partial collapse of the MOF structure is due to the hydrogen bonding of ammonia and/or wa-

ter and the zinc oxide tetrahedra. A decomposition of the MOF network is observed for the copper-based samples as well. Indeed as seen from the X-ray diffraction patterns of HKSUT-1 and the hybrid materials exposed to ammonia, the intensity of the peaks significantly decreased. Unlike in the case of zinc-based materials, for the copper-based samples, this decomposition is likely caused by the formation of complexes between ammonia and the components of HKUST-1. This complexation is evidenced by variations of color of the adsorbents bed during the breakthrough tests. At the beginning of the tests, the bed color changes from dark blue to sky blue. This has already been observed and linked to the binding of ammonia to the copper sites (in axial position) (Britt et al. 2008). Progressively, a new color appears (Maya blue) which indicates the formation of a different copper-based compound. The latter species is hypothesized to be $Cu(OH)_2$ since on the X-ray diffraction pattern of HKUST-1-E and CuMG-2-E, a new peak appears at ∼18° (Liu et al. 2008; Wu et al. 2005).

Information on the water stability of the MOFs can also be derived from the X-ray diffraction patterns (Fig. 9). When MOF-5 is exposed to water, the diffraction pattern is completely altered indicating a collapse of the MOF structure. On the contrary, for HKUST-1, the diffraction pattern is preserved suggesting the water stability. These observations are in agreement with the ones reported in the literature (Kaye et al. 2007; Küsgens et al. 2009). Similar trends as for the parent MOFs are observed for each type of hybrid materials. It can be concluded that the copper-based compounds appear as more sustainable and better candidates for environmental applications.

Further details and support on the mechanisms of adsorption for both series of samples are provided by FT-IR spectroscopy (Fig. 10). The spectrum of the initial GO sample exhibit several bands which can be attributed to the various oxygen and sulfur functionalities present on that material (Petit et al. 2009d). New features, although not well-defined due to the graph's scale, can be observed after exposure to ammonia. A new band at ∼1430 cm^{-1} is seen and assigned to N–H vibration in NH_4^+ (Petit et al. 2009d). The broad overlapping bands between 3100 and 3700 cm^{-1} are attributed to the vibrations of O–H and N–H (Petit et al. 2009d). The other changes in the spectra of GO after exposure to ammonia are related to the modifications in the functional groups of GO after reacting with NH_3 (Petit et al. 2009d). New bands are observed for all exhausted MOFs and hybrid samples. In the case of MOF-5 and the corresponding hybrid materials, new bands appear at 1295, 1220 and 655 cm^{-1}. This is accompanied by more intense bands at 1500 and 1385 cm^{-1} while the initial broad band around 1600 cm^{-1} "is replaced" by a thinner one at 1585 cm^{-1}. The latter changes in the region 1350–1600 cm^{-1} can be attributed to modifications in the coordination of the carboxylate groups from BDC and the zinc centers (Nakamoto 2009). These modifications are likely related to the decomposition of the MOF-5 structure described previously and are similar to the ones observed when MOF-5 is exposed to water. Moreover, N–H vibrations appear at ∼3325 cm^{-1} on MOF-5-E and ZnMG-2-E. Whereas a small band at ∼1700 cm^{-1} is observed on the spectrum of MOF-5 exposed to moist air, this feature is not seen for MOF-5-E and ZnMG-2-E. Since this band is related to the acidic form of BDC, its absence on the latter two samples suggests that ammonia might be interacting with the carboxylate groups of BDC (released by decomposition of the structure) to form $(NH_4)_2$BDC. A similar analysis can be made for HKUST-1 and the corresponding hybrid material. New bands are observed at ∼1620, 1260 and 1210 cm^{-1} and a broadening of the bands at 1450, 1370 and 730 cm^{-1} is seen with and an

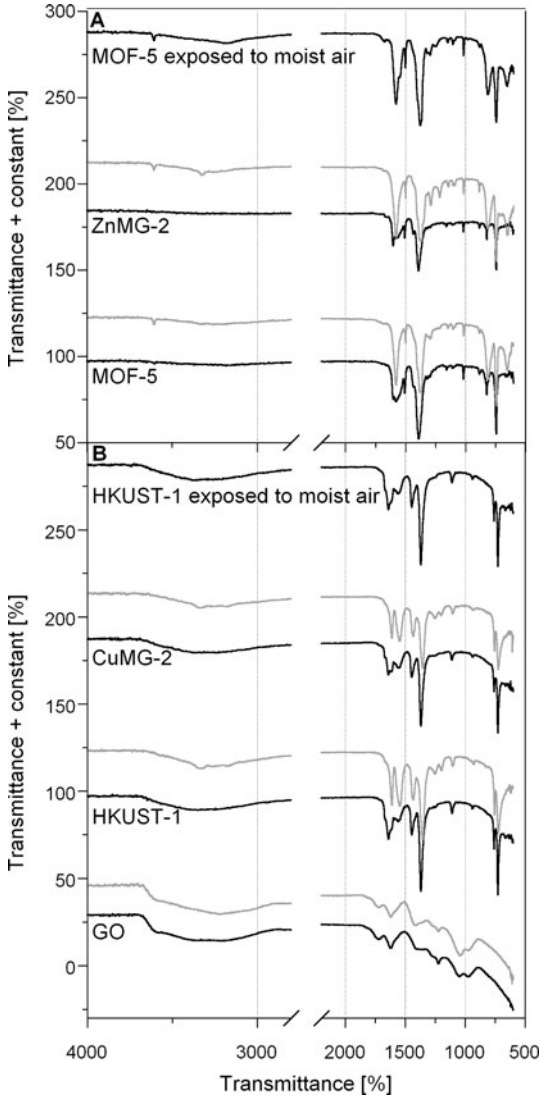

Fig. 10 FT-IR spectra before (*black line*) and after (*gray line*) exposure to ammonia for the (**A**) zinc-based and (**B**) copper-based materials

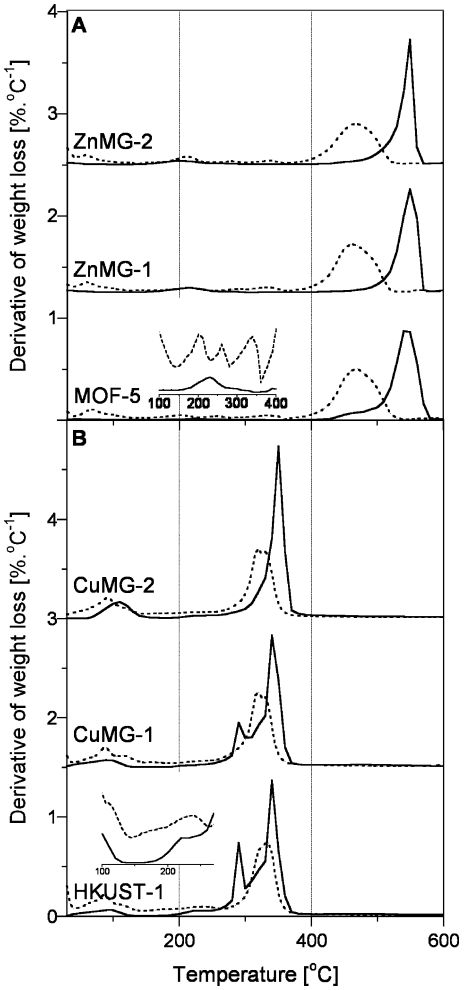

Fig. 11 DTG curves before (*black line*) and after (*gray line*) exposure to ammonia for the (**A**) zinc-based and (**B**) copper-based materials

increase in the intensity of the band at ∼1560 cm^{-1}. The latter feature is assigned to a change in the coordination of the carboxylate ligands from BTC (Nakamoto 2009). Moreover, the appearance of the thin band at ∼1620 cm^{-1} and the ones at ∼1260 and 1210 cm^{-1}, as well as the broadening of the bands at 1370 and 1450 cm^{-1}, suggest the presence of BTC "alone" (not coordinated to copper) (Shi et al. 2008). Once again, the absence of the band at ∼1720 cm^{-1} excludes the presence of the acidic form of BTC (Seo et al. 2009). N–H vibrations are observed at ∼3350 cm^{-1} on HKUST-1-E and CuMG-2-E spectra. Considering all of this, as for the zinc-based materials, the formation of $(NH_4)_3BTC$ is hypothesized.

All of this is supported by the results of thermal analyses (Fig. 11). Decomposition of the MOF structure upon ammonia adsorption is observed for almost all samples via the shift, broadening and decrease of the peak related to the decomposition of BDC (400–550°C for zinc-based compounds) or BTC (300–400°C for copper-based compounds). Moreover, it is interesting to notice that, for the exhausted zinc-based materials, only one broad peak is observed between 400 and 550°C suggesting the decomposition of only one type of species (likely $(NH_4)_2BDC$). On the contrary, for the exhausted copper-based materials, the broad peak between 300–400°C exhibits small shoulders indicating that BTC must be present in different compounds. These compounds can be HKUST-1, $Cu(NH_3)_2BTC_{2/3}$ and $(NH_4)_3BTC$. New peaks are also seen between 150 and 350°C on MOF-5-E (see inset in Fig. 11). This is also observed to a lesser extent for the hybrid materials (not shown here). Similarly, a broad peak is observed between 150 and 270°C on HKUST-1-E (see inset in Fig. 11) and on the hybrid materials too (not shown here). These peaks are likely related to the removal of ammonia and/or the decomposition of $Zn(OH)_2$ for the zinc-based materials and, $Cu(OH)_2$ for the copper-based materials (Lu and Yeh 2000).

4 Conclusions

It is found that the features of the MOF component are dominant in the hybrid materials. Their formation occurs via the coordination of the oxygen groups of GO with the metallic centers of the MOF. The arrangement of GO and the MOF depends on the type of oxygen group involved (from the basal planes or the edges of GO) as well as the geometry of the metallic center. This building process leads to the creation of a new pore space between the MOF blocks and GO with increased dispersive forces. This is responsible for their enhanced adsorption capacities. Overall, better performances are obtained on the copper-based materials than that on the zinc-based materials, which must be related to the presence of unsaturated metallic sites in HKUST-1. Ammonia adsorption causes the collapse of the materials. While in the case of MOF-5 based materials, it is initiated by the hydrogen-bonding of ammonia with the zinc oxide tetrahedra of the MOF, for the copper-based samples, ammonia progressively reacts with the adsorbents via formation of the complexes and leads to their decomposition.

Acknowledgements This study was supported by the ARO (Army Research Office) grant W911NF-05-1-0537 and NSF collaborative grant 0754945/0754979.

References

Biemmi, E., Christian, S., Stock, N., Bein, T.: High throughput screening of synthesis parameters in the formation of the metal-organic frameworks MOF-5 and HKUST-1. Microporous Mesoporous Mater. **117**, 111–117 (2009)

Bissessur, R., Liu, P.K.Y., White, W., Scully, S.F.: Encapsulation of polyanilines into graphite oxide. Langmuir **22**, 1729–1734 (2006)

Britt, D., Tranchemontagne, D., Yaghi, O.M.: Metal-organic frameworks with high capacity and selectivity for harmful gases. Proc. Nat. Acad. Sci. USA **105**, 11623–11627 (2008)

Brodie, M.B.-C.: Note sur un nouveau procede pour la purification et la desagragation du graphite. Ann. Chim. Phys. **45**, 351–353 (1860)

Buchsteiner, A., Lerf, A., Pieper, J.: Water dynamics in graphite oxide investigating by neutron scattering. J. Phys. Chem. B **110**, 22328–22338 (2006)

Chui, S.-Y., Lo, S.M.-F., Charmant, J.P.H., Orpen, A.G., Williams, I.D.: A chemically functionalizable nanoporous material $[Cu_3(TMA)_2(H_2O)_3]_n$. Science **23**, 1148–1150 (1999)

Dubinin, M.M.: In: Walker, P.L. (ed.) Chemistry and Physics of Carbon, vol. 2, pp. 51–120. Dekker, New York (1966)

Greathouse, J.A., Allendorf, M.D.: The interaction of water with MOF-5 simulated by molecular dynamics. J. Am. Chem. Soc. 10678–10679 (2006)

Hafizovic, J., Bjørgen, M., Olsbye, U., Dietzel, P.D.C., Bordiga, S., Prestipino, C., Lamberti, C., Lillerud, K.P.: The inconsistency in adsorption properties and powder XRD data of MOF-5 is rationalized by framework interpenetration and the presence of organic and inorganic species in the nanocavities. J. Am. Chem. Soc. **129**, 3612–3620 (2007)

Huang, L., Wang, H., Chen, J., Wang, Z., Sun, J., Zhao, D., Yan, Y.: Synthesis, morphology control, and properties of porous metal–organic coordination polymers. Microporous Mesoporous Mater. **58**, 105–114 (2003)

Hummers, W.S., Offeman, R.E.: Preparation of graphite oxide. J. Am. Chem. Soc. **8**, 1339 (1958)

Kaye, S.S., Dailly, A., Yaghi, O.M., Long, J.R.: Impact of preparation and handling on the hydrogen storage properties of Zn_4O(1,4-benzenedicarboxylate)$_3$ (MOF-5). J. Am. Chem. Soc. **129**, 14176–14177 (2007)

Konar, S., Mukherjee, P.S., Zangrando, E., Lloret, F., Chaudhuri, N.R.: A Three-dimensional homometallic molecular ferrimagnet. Angew. Chem. Int. Ed. **41**, 1561–1563 (2002)

Küsgens, P., Rose, M., Senkovska, I., Fröde, H., Henschel, A., Siegle, S., Kaskel, S.: Characterization of metal-organic frameworks by water adsorption. Microporous Mesoporous Mater. **20**, 325–330 (2009)

Lerf, A., He, H., Forster, M., Klinowski, J.: Structure of graphite oxide revisited. J. Phys. Chem. B **102**, 4477–4482 (1998)

Li, H., Eddaoudi, M., O'Keeffe, M., Yaghi, O.M.: Design and synthesis of an exceptionally stable and highly porous metal-organic framework. Nature **402**, 276–279 (1999)

Liu, N., Wu, D., Wu, H., Luo, F., Chen, L.: Controllable synthesis of metal hydroxide and oxide nanostructures by ionic liquids assisted electrochemical corrosion method. J. Solid State Sci. **10**, 1049–1055 (2008)

Lu, C.-H., Yeh, C.-H.: Influence of hydrothermal conditions on the morphology and particle size of zinc oxide powder. Ceram. Int. **26**, 351–357 (2000)

Matsuo, Y., Tabata, T.: Preparation and characterization of silylated graphite oxide. Carbon **43**, 2875–2882 (2005)

Morishige, K., Hamada, T.: Iron oxide pillared graphite. Langmuir **21**, 6277–6281 (2005)

Mueller, U., Schubert, M., Teich, F., Puetter, H., Schierle-Arndt, K., Pastré, J.: Metal-organic frameworks—prospective industrial applications. J. Mater. Chem. **16**, 626–636 (2006)

Nakamoto, K.: Complexes of alkoxides, alcohols, ethers, ketones, aldehydes, esters and carboxylic groups. In: Nakamoto, K. (ed.) Infrared and Raman Spectra of Inorganic and Coordination Compounds, pp. 62–67. Wiley, New York (2009)

Park, S., An, J., Jung, I., Piner, R.D., An, S.J., Li, X., Velamakanni, A., Ruoff, R.S.: Colloidal suspensions of highly reduced graphene oxide in a wide variety of organic solvents. Nano Lett. **4**, 1593–1597 (2009)

Pellé, F., Surblé, S., Serre, C., Millange, F., Férey, G., Angew: Enhanced Eu^{3+} luminescence in a new hybrid material with an open-framework structure. J. Lumin. **122–123**, 492–495 (2007)

Petit, C., Bandosz, T.J.: Graphite oxide/polyoxometalate nanocomposites as adsorbents of ammonia. J. Phys. Chem. C **113**, 3800–3809 (2009a)

Petit, C., Bandosz, T.J.: MOF-graphite oxide composites: combining the uniqueness of graphene layers and metal-organic frameworks. Adv. Mater. **21**, 4753–4757 (2009b)

Petit, C., Bandosz, T.J.: Role of surface heterogeneity in the removal of ammonia from air on micro/mesoporous activated carbons modified with molybdenum and tungsten oxides. Microporous Mesoporous Mater. **118**, 61–67 (2009c)

Petit, C., Bandosz, T.J.: Enhanced adsorption of ammonia on metal-organic framework/graphite oxide composites: analysis of surface interactions. Adv. Funct. Mater. **20**, 111–118 (2010a)

Petit, C., Seredych, M., Bandosz, T.J.: Revisiting the chemistry of graphite oxides and its effect on ammonia adsorption. J. Mater. Chem. **19**, 9176–9185 (2009d)

Petit, C., Burress, J., Bandosz, T.J.: Cu-based MOF/graphene composites: synthesis and surface characterization. Carbon (2010b, submitted)

Petit, C., Beacom, B., Bandosz, T.J.: Reactive adsorption of ammonia on Cu-based MOF/graphene composites. Langmuir (2010c, submitted)

Rosi, N.L., Kim, J., Eddaoudi, M., Chen, B., O'Keeffe, M., Yaghi, O.M.: Rod packings and metal-organic frameworks constructed from rod-shaped secondary building units. J. Am. Chem. Soc. **127**, 1504–1518 (2005)

Seo, Y.K., Hundal, G., Jang, I.T., Hwang, Y.K., Jun, C.H., Chang, J.S.: Microwave synthesis of hybrid inorganic–organic materials including porous $Cu_3(BTC)_2$ from Cu(II)-trimesate mixture. Microporous Mesoporous Mater. **119**, 331–337 (2009)

Seredych, M., Petit, C., Tamashausky, A.V., Bandosz, T.J.: Role of graphite precursor in the performance of graphite oxides as ammonia adsorbents. Carbon **47**, 445–456 (2009)

Shi, N., Yin, G., Han, M., Jiang, L., Xu, Z.: Self-assembly of two different hierarchical nanostructures on either side of an organic supramolecular film in one step. Chem. Eur. J. **14**, 6255–6259 (2008)

Stankovich, S., Dikin, D.A., Dommett, G.H.B., Kohlhaas, K.M., Zimney, E.J., Stach, E.A., Piner, R.D., Nguyen, S.T., Ruoff, R.S.: Graphene-based composite materials. Nature **442**, 282–286 (2006)

Stankovich, S., Dikin, D.A., Piner, R.D., Kohlhaas, K.M., Kleinhammes, A., Jia, Y., Wu, Y., Nguyen, S.T., Ruoff, R.S.: Synthesis of graphene-based nanosheets via chemical reduction of exfoliated graphite oxide. Carbon **45**, 1558–1565 (2007)

Stuart, J.: Metal-organic frameworks. Chem. Soc. Rev. **32**, 276–288 (2003)

Szabo, T., Berkesi, O., Forgo, P., Josepovits, K., Sanakis, Y., Petridis, D., Dekany, I.: Evolution of surface functional groups in a series of progressively oxidized graphite oxides. Chem. Mater. **18**, 2740–2749 (2006)

Szymanski, G.S., Karpinski, Z., Biniak, S., Swiatkowski, A.: The effect of the gradual thermal decomposition of surface oxygen species on the chemical and catalytic properties of oxidized activated carbon. Carbon **40**, 2627–2639 (2002)

Wu, X., Bai, H., Zhang, J., Chen, F., Shi, G.: Copper hydroxide nanoneedle and nanotube arrays fabricated by anodization of copper. J. Phys. Chem. B **109**, 22836–22842 (2005)

Yang, S.J., Choi, J.Y., Chae, H.K., Cho, J.H., Nahm, K.S., Park, C.R.: Preparation and enhanced hydrostability and hydrogen storage capacity of CNT@MOF-5 hybrid composite. Chem. Mater. **21**, 1893–1897 (2009)

Yoo, Y., Jeong, H.-K.: Rapid fabrication of metal organic framework thin films using microwave-induced thermal deposition. Chem. Commun. **21**, 2441–2443 (2008)

Yoo, Y., Lai, Z., Ng, Z., Khan, E.A., Jeong, H.-K., Ching, C.-B.: Synthesis of continuous MOF-5 membranes on porous α-alumina substrates. Microporous Mesoporous Mater. **118**, 296–301 (2009)

Zacher, D., Baunemann, A., Hermes, S., Fischer, R.A.: Deposition of microcrystalline $[Cu_3(btc)_2]$ and $[Zn_2(bdc)_2(dabco)]$ at alumina and silica surfaces modified with patterned self assembled organic monolayers: evidence of surface selective and oriented growth. J. Mater. Chem. **17**, 2785–2792 (2007)